Report

Current Biology

# Skin, scales, and cells in a Jurassic plesiosaur

## Highlights

- The first in-depth study of plesiosaur soft tissues is reported
- Some plesiosaurs had smooth skin on the body and small scales on the flippers
- Scales likely enhanced swimming and/or grip on the substrate during feeding

## Authors

Miguel Marx, Peter Sjövall, Benjamin P. Kear, ..., Klaus Nilkens, Michiel Op De Beeck, Johan Lindgren

## Correspondence

miguel.marx@geol.lu.se

## In brief

Marx et al. report the first detailed study of fossilized plesiosaur soft tissues. These show that plesiosaurs possessed both smooth body skin and scaly flippers.

Marx et al., 2025, Current Biology *35*, 1–8
March 10, 2025 
https://doi.org/10.1016/j.cub.2025.01.001

CellPress

Current Biology

CellPress
OPEN ACCESS

Report

# Skin, scales, and cells in a Jurassic plesiosaur

Miguel Marx,[1,7,8,*] Peter Sjövall,[2] Benjamin P. Kear,[3] Martin Jarenmark,[1] Mats E. Eriksson,[1] Sven Sachs,[4] Klaus Nilkens,[5] Michiel Op De Beeck,[6] and Johan Lindgren[1]

[1]Department of Geology, Lund University, Sölvegatan 12, 223 62 Lund, Sweden
[2]RISE Research Institutes of Sweden, Materials and Production, P.O. Box 857, 501 15 Borås, Sweden
[3]The Museum of Evolution, Uppsala University, Norbyvägen 16, 752 36 Uppsala, Sweden
[4]Naturkunde-Museum Bielefeld, Abteilung Geowissenschaften, Adenauerplatz 2, 33602 Bielefeld, Germany
[5]Urwelt-Museum Hauff, Aichelberger Straße 90, 73271 Holzmaden, Germany
[6]Centre for Environmental and Climate Science, Lund University, Sölvegatan 37, 223 62 Lund, Sweden
[7]X (formerly Twitter): @miguelpmarx
[8]Lead contact
*Correspondence: miguel.marx@geol.lu.se
https://doi.org/10.1016/j.cub.2025.01.001

## SUMMARY

Plesiosaurs are an iconic group of Mesozoic marine reptiles with an evolutionary history spanning over 140 million years (Ma).[1] Their skeletal remains have been discovered worldwide; however, accompanying fossilized soft tissues are exceptionally rare.[2] Here, we report a virtually complete plesiosaur from the Lower Jurassic (~183 Ma)[3] Posidonia Shale of Germany that preserves skin traces from around the tail and front flipper. The tail integument was apparently scale-less and retains identifiable melanosomes, keratinocytes with cell nuclei, and the stratum corneum, stratum spinosum, and stratum basale of the epidermis. Molecular analysis reveals aromatic and aliphatic hydrocarbons that likely denote degraded original organics. The flipper integument otherwise integrates small, sub-triangular structures reminiscent of modern reptilian scales. These may have influenced flipper hydrodynamics and/or provided traction on the substrate during benthic feeding. Similar to other sea-going reptiles,[4–10] scalation covering at least part of the body therefore probably augmented the paleoecology of plesiosaurs.

## RESULTS AND DISCUSSION

The classic life reconstruction of plesiosaurs (Plesiosauria), incorporating a long neck, compact body, and four propulsive flippers, has not changed for nearly 200 years.[1,11] However, the actual external appearance of these famous Mesozoic reptiles is largely unknown. Recent comprehensive microscopic and spectroscopic analyses of fossilized soft tissues have shed light on the paleoecology and evolution of other extinct marine reptiles.[10,12–17] By contrast, with only eight plesiosaur soft tissue specimens scientifically documented to date,[2,18–24] the extreme rarity of such non-skeletal remains has hindered equivalent studies.

Here, we report a well-preserved plesiosaur (Urwelt-Museum Hauff, Holzmaden, Germany [MH] 7) from the world-renowned Lower Jurassic (Lias $\varepsilon II_{6C}$, lower Toarcian[25,26]) Posidonia Shale (Posidonienschiefer Formation) of southern Germany. MH 7 was excavated from a quarry near Holzmaden in 1940. Preparation of the skeleton in 2020 uncovered soft tissue traces from around the tail and trailing edge of the right forelimb (Figure 1A). We therefore applied a suite of techniques, including transmitted light microscopy (TLM), scanning electron microscopy (SEM), energy-dispersive X-ray spectroscopy (EDX), electron backscatter diffraction (EBSD), infrared (IR) microspectroscopy, and time-of-flight secondary ion mass spectrometry (ToF-SIMS) to examine MH 7 in unprecedented detail.

### Description and analysis

The fossilized soft tissues of MH 7 (Figures 1, 2, and 3) are mainly exposed along the dorsal and ventral sides of the caudal vertebral column (Figures 1B and 1C) and behind the bones of the right forelimb. Small patches also cover the ends of some caudal ribs, the caudal neural spines, and distal phalanges. We identify these soft tissue remains as skin based on the presence of a distinct internal layering that morphologically corresponds to the stratum corneum, stratum spinosum, and stratum basale of the integument in living amniotes.[27–29]

The stratum spinosum of the tail skin in MH 7 is up to ~215 μm thick, whereas the stratum corneum is relatively thin (~15–25 μm). Fossil keratinocytes are observable within the stratum spinosum. These are ~20 μm in diameter and sub-circular in outline, with dark centers that we interpret as remnant cell nuclei (Figures 1D and 1E). The preserved keratinocytes become flattened toward the external surface of the skin (facing into the sediment matrix) and are thus consistent with corneocytes (enucleated keratinocytes), which comprise the stratum corneum in modern reptiles (Figure 1F). Clusters of dark-colored melanosome microbodies derived from decayed melanophores are also dispersed through the outer skin layers (Figures 1G and 1H). In addition, the stratum basale is demarcated by columnar keratinocytes (Figures 1I and 1J).

Voids occur throughout the stratum spinosum where keratinocytes are not preserved. EDX of petrographic thin-sections detected predominantly calcium and phosphorus in the stratum

Please cite this article in press as: Marx et al., Skin, scales, and cells in a Jurassic plesiosaur, Current Biology (2025), https://doi.org/10.1016/j.cub.2025.01.001



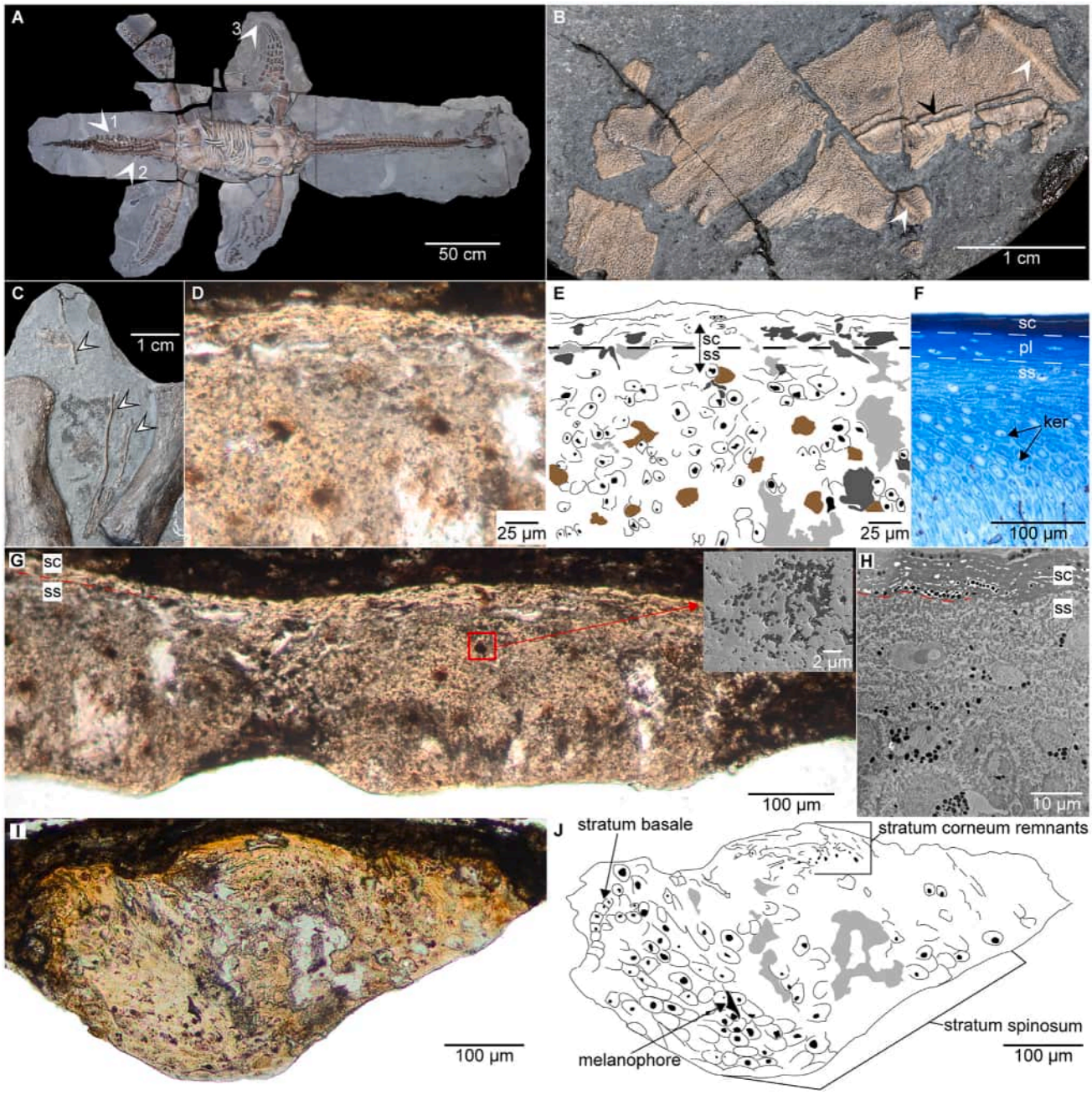


**Figure 1. Plesiosaur specimen (MH 7) with comparisons**

(A) MH 7 in ventral view, showing soft tissue sampling sites (arrows) on the dorsal (1) and ventral side (2) of the tail and trailing edge (3) of the right front flipper.
(B) Skin from the ventral side of the tail showing thick folds (white arrows) and an apparently torn surface (black arrow).
(C) Skin from the dorsal side of the tail (white arrows).
(D and E) (D) TLM image of skin from (B) with diagram (E), showing the differentiated stratum corneum (sc) and underlying stratum spinosum (ss), keratinocytes with cell nuclei (circular structures with black dots), melanosome aggregates (brown patches), voids (light gray patches), and indeterminate organics or minerals (dark gray patches).
(F) Comparative thin-section through the eyelid epidermis of an extant Leatherback turtle, *Dermochelys coriacea*, indicating the similarly differentiated sc, pre-corneous layer (pl), ss, and keratinocytes (ker).
(G) TLM image of a petrographic thin-section showing skin from the ventral side of the tail in MH 7. Inset: SEM image enlargement of ellipsoidal melanosome microbodies (red box).
(H) TEM image of carapace skin from *D. coriacea*, showing differentiated sc and ss, including melanosomes (dark dots).
(I and J) (I) TLM image with diagram (J) showing a petrographic thin-section of skin from the dorsal side of the tail in MH 7 incorporating the sc, ss with a remnant melanophore, and the stratum basale.

Please cite this article in press as: Marx et al., Skin, scales, and cells in a Jurassic plesiosaur, Current Biology (2025), https://doi.org/10.1016/j.cub.2025.01.001



CellPress
OPEN ACCESS

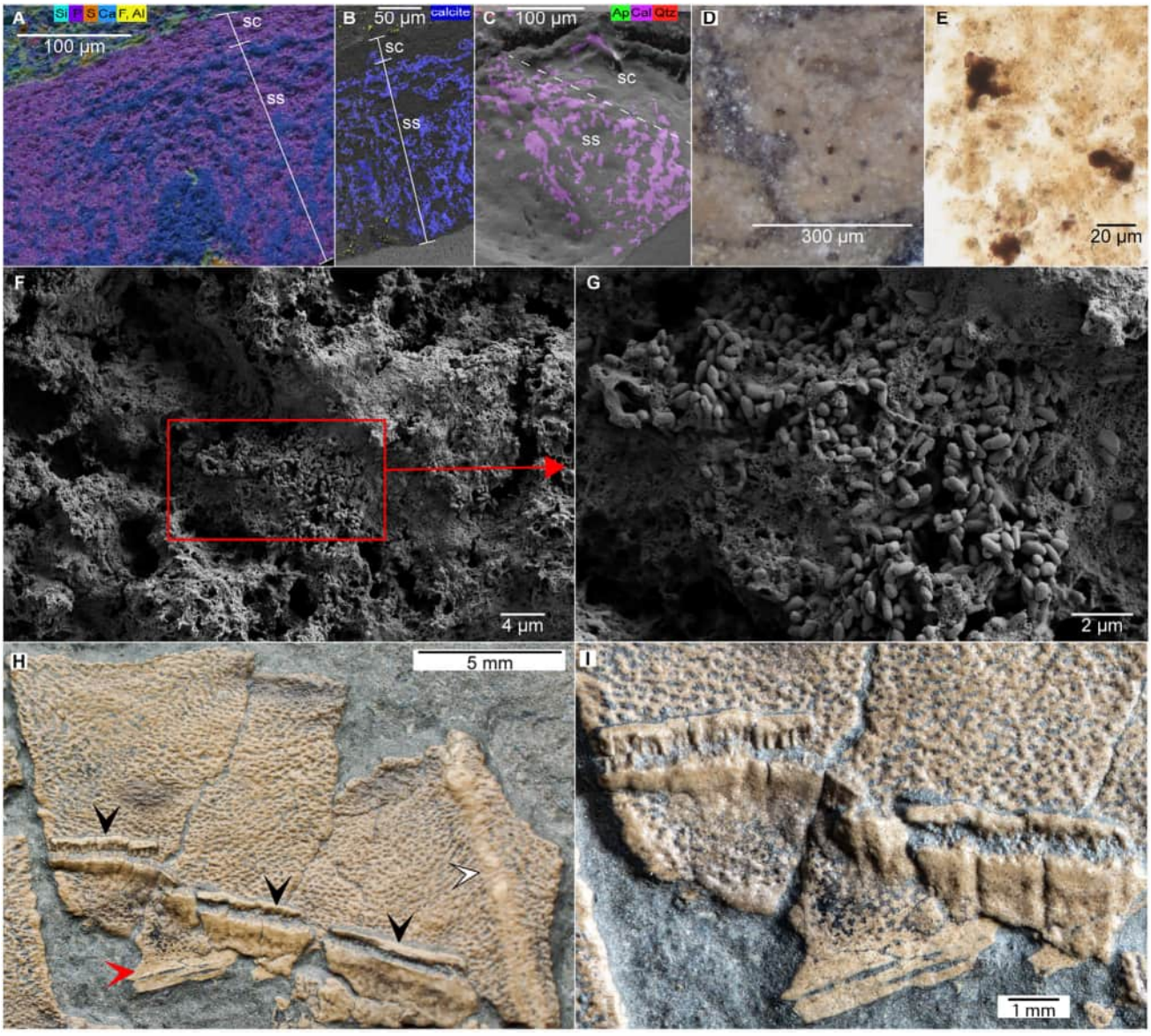


**Figure 2. Plesiosaur tail skin**

(A) EDX elemental map of a petrographic thin-section through skin from the ventral side of the tail in MH 7, indicating the phosphorus (P)-rich sc and P/calcium (Ca)-rich ss. Colors: cyan, silicon (Si); purple, P; orange, sulfur (S); blue, Ca; yellow, fluorine/aluminum (F, Al).

(B) EBSD map of (A). Color: blue, calcite (Cal).

(C) EBSD map of skin from the dorsal side of the tail, showing the ss permeated with Cal. Colors: green, apatite (Ap); purple, Cal; red, quartz (Qtz).

(D and E) (D) Light microscopy (LM) image of skin from the ventral side of the tail in MH 7 showing clusters of melanosome microbodies (dark dots) with TLM image of the same skin after demineralization (E).

(F and G) (F) SEM image of demineralized skin from the ventral side of the tail in MH 7 with enlargement (G) of melanosome microbodies.

(H and I) (H) Skin from the ventral side of the tail showing pitted ss with apparent folding (white arrow) and tearing (black arrows). Smooth areas of the ss (red arrow); (I) enlargement of possible torn skin from (H).

See also Figures S3 and S4.

spinosum, whereas the stratum corneum is enriched with phosphorus but lacks calcium (Figure 2A). EBSD similarly found calcite in the stratum spinosum but little or no calcite in the stratum corneum (Figures 2B and 2C). This distribution implies progressive mineralization from the exterior to interior of the skin and, presumably, involved calcium phosphate replication of the stratum corneum versus partial replacement of the stratum spinosum by calcium phosphate and, later, calcite that filled voids left by more advanced decay.

Ellipsoidal melanosome microbodies are evident within the tail skin of MH 7 after demineralization (Figures 2D–2G). The internal skin surface (facing away from the sediment matrix) is covered by irregular pits and what appear to be thickened folds (Figure 2H). Several overlying skin fragments were

Please cite this article in press as: Marx et al., Skin, scales, and cells in a Jurassic plesiosaur, Current Biology (2025), https://doi.org/10.1016/j.cub.2025.01.001



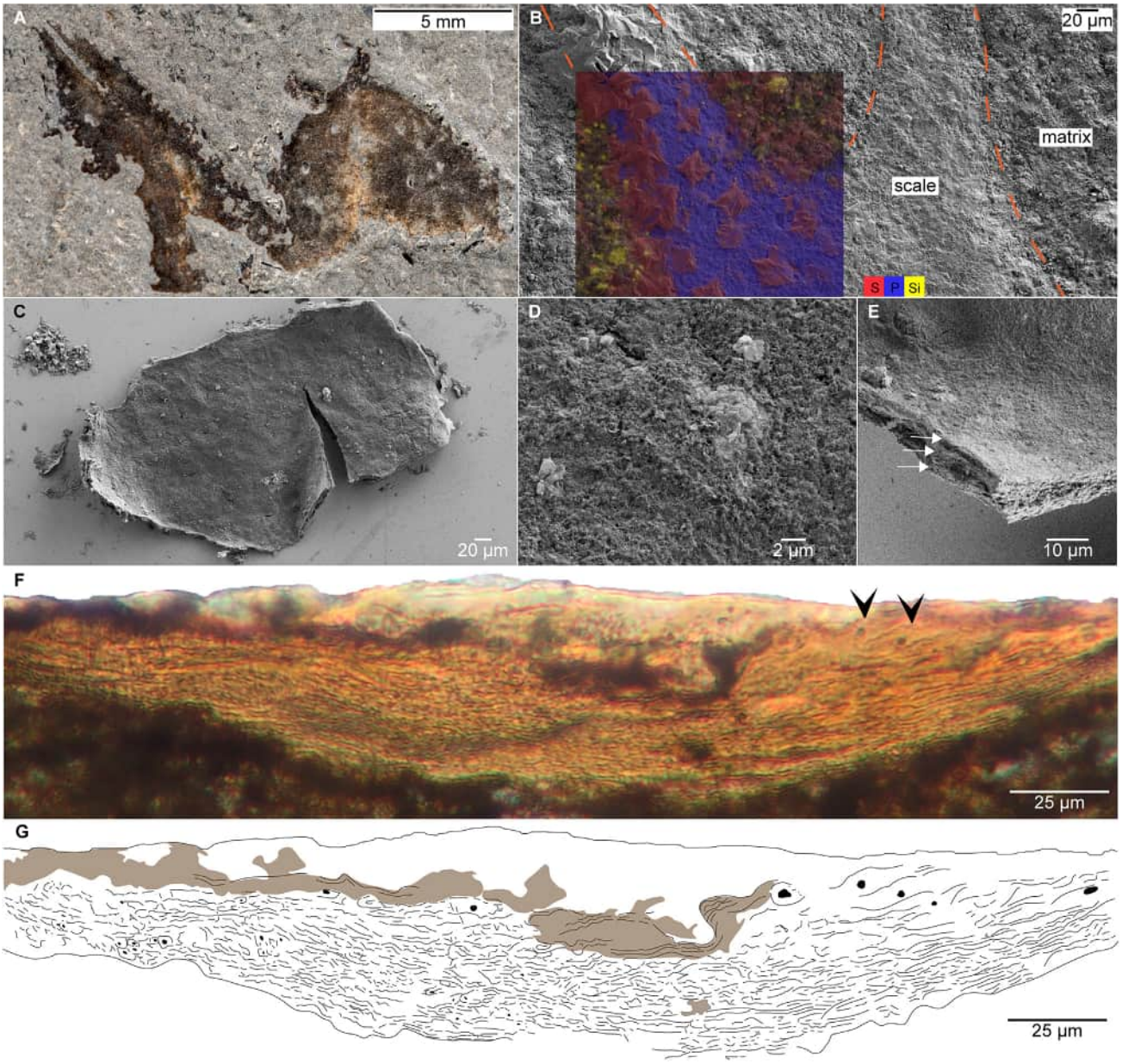


**Figure 3. Plesiosaur flipper scales**

(A) Scales from the trailing edge of the right flipper in MH 7 (see Figure 1A), showing their irregularly sub-triangular shape and light-colored midline sediment infill.
(B) SEM image with inset EDX elemental map (orange dashed line: scale boundary). Colors: red, S; blue, P; yellow, Si.
(C) SEM image of demineralized scale fragment from MH 7 showing a smooth surface.
(D) Enlarged SEM image showing absence of melanosome microbodies on the scale surface of MH 7.
(E) SEM image of the scale margin from MH 7 showing internal layering (white arrows).
(F and G) (F) TLM image with diagram (G) of a petrographic thin-section through the scaly flipper skin from MH 7 showing ker (black arrows), cell nuclei (black dots), and the outermost dense corneocyte layer (brown fill) covered by mineral deposits (white fill).
See also Figures S1 and S2.

seemingly torn to expose an interdigitating ''zig-zagged'' texture (Figure 2I).

By contrast, skin from the right forelimb incorporates small and irregularly sub-triangular structures that we recognize as scales (Figure 3A). These were coated in sulfur precipitates prior to demineralization (Figure 3B) but retained structural integrity after demineralization to reveal smooth surfaces that lack melanosomes (Figures 3C and 3D). They clearly differ from the soft, scale-less skin occurring around the tail of MH 7 and instead compare closely with carapace scutes of fossil and living turtles (Figures S1A and S1B), as well as mosasauroid marine lizard scales (Figures S1C and S1D), which can similarly exhibit

Please cite this article in press as: Marx et al., Skin, scales, and cells in a Jurassic plesiosaur, Current Biology (2025), https://doi.org/10.1016/j.cub.2025.01.001





sediment infilling along their midline, exposed by erosion of the longitudinal keel[7] (contrary to smooth ichthyosaur skin; Figure S1E). Diagnostically, the stratified edges of the scales in MH 7 (Figure 3E) have a thick (~36 μm) outermost corneocyte layer (Figures 3F and 3G) that is identical to the tough stratum corneum characterizing the scaly skin of modern reptiles.[30–32]

Our ToF-SIMS analyses (Figures S2 and S3) detected polycyclic aromatic hydrocarbons (PAHs) and aliphatic hydrocarbons indicative of asphaltene-like molecular structures in the tail and flipper skin of MH 7. Eumelanin was not identified, and may have been diagenetically transformed into PAH-like compounds during fossilization. IR spectra also produced peaks attributable to hydrocarbons: 1,378 $cm^{-1}$ ($\delta_s$ ($CH_3$)) and 1,458 $cm^{-1}$ ($\delta_{as}$ ($CH_3$) $\delta_s$ ($CH_2$)) (C–H distortion)[15]; 1,714 $cm^{-1}$ ($\nu$(C=O))[33]; 2,852 and 2,923 $cm^{-1}$ (C–H stretches).[15] Peaks in the ~1,000 to ~1,100 $cm^{-1}$ region correspond to the phosphate ($PO_4^{-3}$) group[15,34] (Figure S4).

## Interpretations of plesiosaur skin

The body of MH 7 was seemingly covered in a mosaic of smooth skin and (possibly keeled) scales like some turtles.[10] Indeed, the epidermal microstructure of MH 7 corresponds well to that of living amniotes, with an outermost stratum corneum comprising compacted corneocytes and an underlying stratum spinosum composed of younger, sub-spherical skin cells.[27–29]

Frey et al.[2] suggested that the rarity of recovered plesiosaur skin might be due to their epidermis being thin, as in extant snakes,[35] and thus susceptible to rapid breakdown after death. Conversely, the combined depth of the stratum spinosum and stratum corneum in MH 7 (which was at least ~250 μm) implies a thick epidermis, more compatible with that of living sea turtles (Figures S1F and S1G). The low preservation potential of plesiosaur skin in the Posidonia Shale could, therefore, be a consequence of their infrequent burial in dysoxic seafloor deposits conducive to soft tissue fossilization[24,36] or because their skin remnants were unintentionally removed during mechanical/chemical preparation.

Melanophore traces are situated close to the outer surface of the tail skin in MH 7, which contrasts with many modern reptiles, where pigment cells are typically concentrated in the deep epidermis and superficial dermis.[37,38] However, epidermal pigment cells can also be located just below (but not within) the stratum corneum,[30] thereby potentially explaining the pigment cell arrangement that we observe in MH 7.

The flipper skin of MH 7 is otherwise very similar to that of modern scaly reptiles.[32,39] In particular, the outer corneocyte layer is devoid of melanophore traces and substantially thicker than that of the scale-less skin from around the tail. This difference is expected because the highly keratinized outermost epidermis of reptilian scales usually comprises a deep layer of compacted corneocytes[40] (Figure S1H). These cells are characterized by corneous beta-proteins that make living reptile scales hard and immobile.[41] Yet, our ToF-SIMS analyses failed to detect any residual proteinaceous matter, probably because the molecular content of MH 7 was completely transformed by diagenetic processes during fossilization.

## Functional roles of plesiosaur skin

In conjunction with MH 7, we examined other Posidonia Shale plesiosaurs that preserve soft tissue remains. The most informative were specimens of the microcleidids (Microcleididae) *Seeleyosaurus guilelmiimperatoris* (Museum für Naturkunde Berlin, Germany [MB].R.1992) and *Microcleidus brachypterygius* (Paläontologische Sammlung, Universität Tübingen, Germany [GPIT]-PV-30094). These complete skeletons exhibit associated integument remnants (incorporating dark, presumably melanic residues and embedded "fibrous structures"[15,17,42,43]) behind the bones of the forelimbs (Figures 4A–4C). Such tissue traces derive from the flexible trailing edge of the flippers that served to generate thrust as hydrofoils in underwater flight.[44,45] Our novel detection of scales on the flipper of MH 7 might, therefore, imply a hydrodynamic function because these integumentary appendages may have stiffened the trailing edge during swimming.[9,10] Not surprisingly, soft tissue trailing edges have also been reported on the hindlimb hydrofoils[46] of Posidonia Shale microcleidids (Staatliches Museum für Naturkunde Stuttgart, Germany [SMNS] 51945)[24] and in the Late Cretaceous short-necked polycotylid (Polycotylidae) *Mauriciosaurus fernandezi*, which purportedly possessed scale rows along the body[2] (although these could be artifacts of taphonomic deformation and/or cracking). Furthermore, MB.R. 1992 has a large, fleshy tail fin (Figures 4D and 4E) that was either vertically[19,47] or horizontally[48] oriented and potentially acted as a rudder for maneuverability[47] or to facilitate caudally driven propulsion.[48]

Another purpose of the flipper scales in MH 7 may have been to provide a protective covering for traction on the seafloor during benthic "grazing." This is consistent with plesiosaur "bottom-walking"[49,50] and feeding traces,[51] as well as preserved gastric contents,[24,52] which comprise coarse sediment masses in SMNS 51945[24] and MB.R.1992—the latter individual had also swallowed a mixture of small gastropods and cephalopods (Figures 4F and 4G). Extant sea turtles[53] and dolphins[54] likewise ingest large volumes of sand and mud when sifting through seafloor sediments for prey.

In summary, our comprehensive morphological, microscopic, and spectroscopic investigation of the soft tissue residues in MH 7 suggests that plesiosaurs (and more basal sauropterygians[22]) retained reptilian scaly skin throughout their land-to-sea transition and later specialization for life in the open ocean. This contrasts with other Mesozoic marine reptiles, including ichthyosaurs[15,55] and metriorhynchid crocodylomorphs,[56] which lost or reduced their scalation to reduce drag. Although the scale-less tail skin of MH 7 hints at an analogous external body appearance, the presence of at least partial squamation along the trailing edges of the flippers undoubtedly fulfilled some functional role and presumably conferred a selective advantage for plesiosaurs during their protracted evolution as one of the most successful pelagic tetrapod clades.

## RESOURCE AVAILABILITY

### Lead contact

Further information and requests for resources and reagents should be directed to and will be fulfilled by the lead contact, Miguel Marx (miguel.marx@geol.lu.se).

### Materials availability

This study did not generate new unique reagents.

Please cite this article in press as: Marx et al., Skin, scales, and cells in a Jurassic plesiosaur, Current Biology (2025), https://doi.org/10.1016/j.cub.2025.01.001



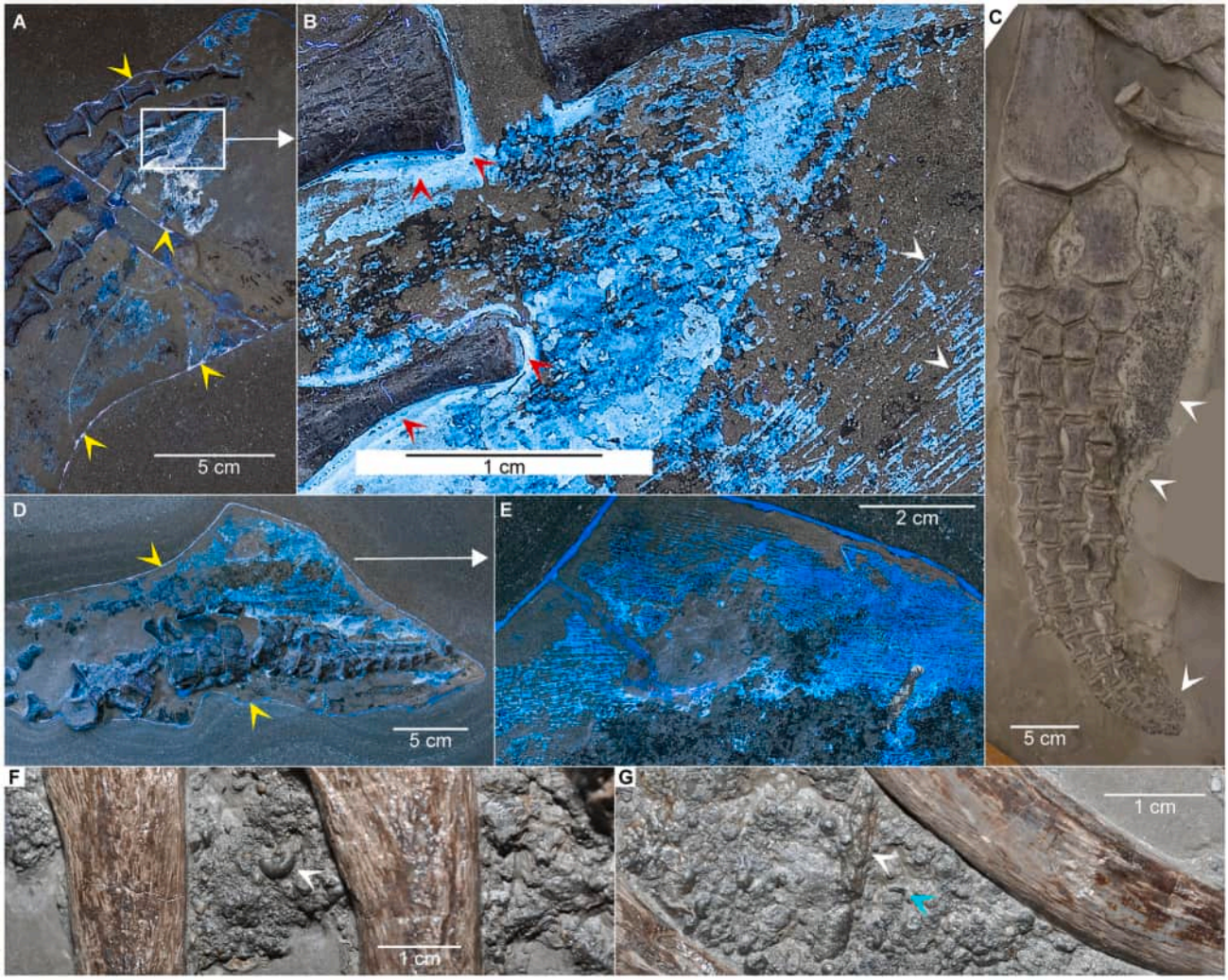


**Figure 4. Plesiosaur soft tissues and gut contents**

(A) UV image (cutoff at ~365 nm) of soft tissues and glued edges (yellow arrows) from the trailing edge of the right flipper in *Seeleyosaurus guilelmiimperatoris* (MB.R.1992). White box indicates enlargement (B).

(B) Enlargement from (A) showing skin traces with embedded 3D "fibrous structures"[15,17,42,43] (white arrows) and surrounding glue (red arrows).

(C) Left forelimb trailing edge (white arrows) of *Microcleidus brachypterygius* (GPIT-PV-30094).

(D) UV image (cutoff at ~365 nm) of the incomplete and partially restored[19,47,48] (yellow arrows) tail fin from *S. guilelmiimperatoris* (MB.R.1992).

(E) Enlargement from (D) showing fibrous structures.[15,17,42,43]

(F) Preserved gut contents from *S. guilelmiimperatoris* (MB.R.1992), comprising a coarse sediment mass with a gastropod shell (white arrow).

(G) Possible belemnite phragmocone/guard (white arrow) and onychite (arm hook: cyan arrow) within the preserved gut contents from *S. guilelmiimperatoris* (MB.R.1992).

## Data and code availability

MH 7 is accessioned and permanently housed in the publicly accessible collection at MH. All experimental samples derived from MH 7 are stored at the Department of Geology, Lund University (LU), Sweden. Any information required to reanalyze the data reported in this paper is available from the lead contact upon request.

## ACKNOWLEDGMENTS

We thank R. Hauff, F. Hauff, B. Hauff, and A. Fichtner (MH); O. Hampe and S. Thiel (MB); I. Werneburg and A. Krahl (GPIT); E.E. Maxwell (SMNS); R.M. Carney (University of South Florida); D.K. Johansson (University of Copenhagen Zoological Museum); and D.A. Winkler and M.J. Polcyn (Southern Methodist University) for access to specimens and information, and for their hospitality during our research visits. F. Hauff contributed to the editing. C. Sandt assisted with IR microspectroscopy. F. Borondics prepared samples for SMIS analysis at SOLEIL. C. Alwmark, G. Zachén, J. Martell, and A. Plan contributed to SEM, EDX, and EBSD data processing. H.J. Götz (MB) took UV photographs of MB.R.1992. O. Gustafsson and C. Rasmussen provided information on histological samples. Financial support included Swedish Research Council grants to J.L. (2020-03542), B.P.K. (2020-03423), P.S. (2019-03731), and M.E.E. (2019-03516). M.M. also acknowledges travel funding from the Royal Physiographic Society of Lund (42011).

## AUTHOR CONTRIBUTIONS

Conceptualization, M.M., J.L., B.P.K., and S.S.; methodology, M.M., J.L., P.S., M.J., and M.O.D.B.; investigation, M.M., J.L., P.S., and M.O.D.B.; writing – original

draft, M.M.; writing – review and editing, B.P.K., M.M., J.L., M.E.E., M.J., S.S., K.N., and M.O.D.B.; visualization, M.M., P.S., and K.N.; funding acquisition, J.L., B.P.K., M.E.E., P.S., and M.M.

## DECLARATION OF INTERESTS

The authors declare no competing interests.

## STAR★METHODS

Detailed methods are provided in the online version of this paper and include the following:

- KEY RESOURCES TABLE
- METHOD DETAILS
  - Sample preparation
  - TLM and thin-sectioning
  - SEM, EDX, and EBSD
  - IR microspectroscopy and ToF-SIMS
  - Comparative samples

## SUPPLEMENTAL INFORMATION

Supplemental information can be found online at https://doi.org/10.1016/j.cub.2025.01.001.

Received: March 15, 2024
Revised: October 28, 2024
Accepted: January 3, 2025
Published: February 6, 2025

## REFERENCES

1. Sander, P.M. (2023). Plesiosaurs. Curr. Biol. *33*, R389–R396.
2. Frey, E., Mulder, E.W.A., Stinnesbeck, W., Rivera-Sylva, H.E., Padilla-Gutiérrez, J.M., and González-González, A.H. (2017). A new polycotylid plesiosaur with extensive soft tissue preservation from the early Late Cretaceous of northeast Mexico. Bol. Soc. Geol. Mex. *69*, 87–134.
3. van Acken, D., Tütken, T., Daly, J.S., Schmid-Röhl, A., and Orr, P.J. (2019). Rhenium-osmium geochronology of the Toarcian Posidonia Shale, SW Germany. Palaeogeogr. Palaeoclimatol. Palaeoecol. *534*, 109294.
4. Renesto, S.C., and Avanzini, M. (2002). Skin remains in a juvenile *Macrocnemus bassanii* Nopcsa (Reptilia, Prolacertiformes) from the Middle Triassic of northern Italy. N. Jahrb. Geol. Paläontol. Abh. *224*, 31–48.
5. Caldwell, M.W., and Dal Sasso, C.D. (2004). Soft-tissue preservation in a 95 million year old marine lizard: form, function, and aquatic adaptation. J. Vertebr. Paleontol. *24*, 980–985.
6. Renesto, S. (2005). A new specimen of *Tanystropheus* (Reptilia Protorosauria) from the Middle Triassic of Switzerland and the ecology of the genus. Riv. Ital. Paleontol. Stratigr. *111*, 377–394.
7. Lindgren, J., Alwmark, C., Caldwell, M.W., and Fiorillo, A.R. (2009). Skin of the Cretaceous mosasaur *Plotosaurus*: implications for aquatic adaptations in giant marine reptiles. Biol. Lett. *5*, 528–531.
8. Lindgren, J., Caldwell, M.W., Konishi, T., and Chiappe, L.M. (2010). Convergent evolution in aquatic tetrapods: insights from an exceptional fossil mosasaur. PLoS One *5*, e11998.
9. Joyce, W.G., Mäuser, M., and Evers, S.W. (2021). Two turtles with soft tissue preservation from the platy limestones of Germany provide evidence for marine flipper adaptations in Late Jurassic thalassochelydians. PLoS One *16*, e0252355.
10. De La Garza, R.G., Madsen, H., Sjövall, P., Osbæck, F., Zheng, W., Jarenmark, M., Schweitzer, M.H., Engdahl, A., Uvdal, P., Eriksson, M.E., et al. (2022). An ancestral hard-shelled sea turtle with a mosaic of soft skin and scutes. Sci. Rep. *12*, 22655.
11. de Blainville, H.D. (1835). Description de quelques espèces de reptiles de la Californie, précédée de l'analyse d'un système général d'Erpétologie et d'Amphibiologie. Nouv. Ann. Mus. Hist. Nat., Paris *4*, 233–296.
12. Lindgren, J., Kaddumi, H.F., and Polcyn, M.J. (2013). Soft tissue preservation in a fossil marine lizard with a bilobed tail fin. Nat. Commun. *4*, 2423.
13. Lindgren, J., Sjövall, P., Carney, R.M., Uvdal, P., Gren, J.A., Dyke, G., Schultz, B.P., Shawkey, M.D., Barnes, K.R., and Polcyn, M.J. (2014). Skin pigmentation provides evidence of convergent melanism in extinct marine reptiles. Nature *506*, 484–488.
14. Lindgren, J., Kuriyama, T., Madsen, H., Sjövall, P., Zheng, W., Uvdal, P., Engdahl, A., Moyer, A.E., Gren, J.A., Kamezaki, N., et al. (2017). Biochemistry and adaptive colouration of an exceptionally preserved juvenile fossil sea turtle. Sci. Rep. *7*, 13324.
15. Lindgren, J., Sjövall, P., Thiel, V., Zheng, W., Ito, S., Wakamatsu, K., Hauff, R., Kear, B.P., Engdahl, A., Alwmark, C., et al. (2018). Soft-tissue evidence for homeothermy and crypsis in a Jurassic ichthyosaur. Nature *564*, 359–365.
16. De La Garza, R.G., Madsen, H., Eriksson, M.E., and Lindgren, J. (2021). A fossil sea turtle (Reptilia, Pan-Cheloniidae) with preserved soft tissues from the Eocene Fur Formation of Denmark. J. Vertebr. Paleontol. *41*, e1938590.
17. De La Garza, R.G., Sjövall, P., Hauff, R., and Lindgren, J. (2023). Preservational modes of some ichthyosaur soft tissues (Reptilia, Ichthyopterygia) from the Jurassic Posidonia Shale of Germany. Palaeontol. *66*, e12668.
18. Sollas, W.J. (1881). On a new species of *Plesiosaurus* (*P. conybeari*) from the Lower Lias of Charmouth; with observations on *P. megacephalus*, Stutchbury, and *P. brachycephalus*, Owen. Q. J. Geol. Soc. *37*, 440–481.
19. Dames, W.B. (1895). Die Plesiosaurier der süddeutschen Liasformation (Abhandlungen der Königlich Preussischen Akademie der Wissenschaften Zu Berlin), pp. 1–81.
20. Watson, D.M.S. (1911). The Upper Liassic Reptilia. Part III: *Microcleidus macropterus* (Seeley) and the limbs of *Microcleidus homalospondylus* (Owen). Mem. Manch. Lit. Philos. Soc. *55*, 1–9.
21. von Huene, F. (1923). Ein neuer Plesiosaurier aus dem oberen Lias Württembergs. Jahreshefte Des Vereins für Vaterländische Naturkunde in Württemberg *79*, 3–23.
22. Sander, P.M. (1989). The pachypleurosaurids (Reptilia: Nothosauria) from the Middle Triassic of Monte San Giorgio (Switzerland) with the description of a new species. Philos. Trans. R. Soc. Lond. B Biol. Sci. *325*, 561–666.
23. Sachs, S., Hornung, J.J., and Kear, B.P. (2016). Reappraisal of Europe's most complete Early Cretaceous plesiosaurian: *Brancasaurus brancai* Wegner, 1914 from the "Wealden facies" of Germany. PeerJ *4*, e2813.
24. Vincent, P., Allemand, R., Taylor, P.D., Suan, G., and Maxwell, E.E. (2017). New insights on the systematics, palaeoecology and palaeobiology of a plesiosaurian with soft tissue preservation from the Toarcian of Holzmaden, Germany. Naturwissenschaften *104*, 51.
25. Hauff, B. (1921). Untersuchungern der Fossilfundstätten von Holzmaden im Posidonienschiefer des Oberen Lias Württembergs. Palaeontograph. *64*, 1–41.
26. Röhl, H.-J., Schmid-Röhl, A., Oschmann, W., Frimmel, A., and Schwark, L. (2001). The Posidonia Shale (Lower Toarcian) of SW-Germany: an oxygen-depleted ecosystem controlled by sea level and palaeoclimate. Palaeogeogr. Palaeoclimatol. Palaeoecol. *165*, 27–52.
27. Dubansky, B.H., and Close, M. (2019). A review of alligator and snake skin morphology and histotechnical preparations. J. Histotechnol. *42*, 31–51.
28. Cowan, M.L., Raidal, S.R., and Peters, A. (2015). Herpesvirus in a captive Australian Krefft's river turtle (*Emydura macquarii krefftii*). Aust. Vet. J. *93*, 46–49.
29. Abramo, F., Campora, L., Albanese, F., della Valle, M.F., Cristino, L., Petrosino, S., Di Marzo, V., and Miragliotta, V. (2014). Increased levels of palmitoylethanolamide and other bioactive lipid mediators and enhanced local mast cell proliferation in canine atopic dermatitis. BMC Vet. Res. *10*, 21.

30. Alibardi, L. (2011). Histology, ultrastructure, and pigmentation in the horny scales of growing crocodilians. Acta Zool. *92*, 187–200.
31. Alibardi, L. (2013). Observations on the ultrastructure and distribution of chromatophores in the skin of chelonians. Acta Zool. *94*, 222–232.
32. Kandyel, R.M., Elwan, M.M., Abumandour, M.M.A., and El Nahass, E.E. (2021). Comparative ultrastructural-functional characterizations of the skin in three reptile species; *Chalcides ocellatus*, *Uromastyx aegyptia aegyptia*, and *Psammophis schokari aegyptia* (FORSKAL, 1775): adaptive strategies to their habitat. Microsc. Res. Tech. *84*, 2104–2118.
33. Ulagappan, N., and Frei, H. (2000). Mechanistic study of $CO_2$ photoreduction in Ti silicalite molecular sieve by FT-IR spectroscopy. J. Phys. Chem. A *104*, 7834–7839.
34. Mobasherpour, I., Heshajin, M.S., Kazemzadeh, A., and Zakeri, M. (2007). Synthesis of nanocrystalline hydroxyapatite by using precipitation method. J. Alloys Compd. *430*, 330–333.
35. Shine, R., Goiran, C., Shilton, C., Meiri, S., and Brown, G.P. (2019). The life aquatic: an association between habitat type and skin thickness in snakes. Biol. J. Linn. Soc. *128*, 975–986.
36. Muscente, A.D., Vinnes, O., Sinha, S., Schiffbauer, J.D., Maxwell, E.E., Schweigert, G., and Martindale, R.C. (2023). What role does anoxia play in exceptional fossil preservation? Lessons from the taphonomy of the Posidonia Shale (Germany). Earth Sci. Rev. *238*, 104323.
37. Kuriyama, T., Miyaji, K., Sugimoto, M., and Hasegawa, M. (2006). Ultrastructure of the dermal chromatophores in a lizard (Scincidae: *Plestiodon latiscutatus*) with conspicuous body and tail coloration. Zoolog. Sci. *23*, 793–799.
38. Kuriyama, T., Murakami, A., Brandley, M., and Hasegawa, M. (2020). Blue, black, and stripes: evolution and development of color production and pattern formation in lizards and snakes. Front. Ecol. Evol. *8*, 232.
39. Chang, C., Wu, P., Baker, R.E., Maini, P.K., Alibardi, L., and Chuong, C.M. (2009). Reptile scale paradigm: Evo-Devo, pattern formation and regeneration. Int. J. Dev. Biol. *53*, 813–826.
40. Alibardi, L. (2023). Scales of non-avian reptiles and their derivatives contain corneous beta proteins coded from genes localized in the Epidermal Differentiation Complex. Tissue Cell *85*, 102228.
41. Alibardi, L. (2016). Sauropsids cornification is based on corneous beta-proteins, a special type of keratin-associated corneous proteins of the epidermis. J. Exp. Zool. B Mol. Dev. Evol. *326*, 338–351.
42. Lingham-Soliar, T. (1999). Rare soft tissue preservation showing fibrous structures in an ichthyosaur from the Lower Lias (Jurassic) of England. Proc. R. Soc. Lond. B. Biol. Sci. *266*, 2367–2373.
43. Lingham-Soliar, T., and Wesley-Smith, J. (2008). First investigation of the collagen D-band ultrastructure in fossilized vertebrate integument. Proc. R. Soc. Lond. B. Biol. Sci. *275*, 2207–2212.
44. Krahl, A., and Witzel, U. (2021). Foreflipper and hindflipper muscle reconstructions of *Cryptoclidus eurymerus* in comparison to functional analogues: introduction of a myological mechanism for flipper twisting. PeerJ *9*, e12537.
45. DeBlois, M.C., and Motani, R. (2019). Flipper bone distribution reveals flexible trailing edge in underwater flying marine tetrapods. J. Morphol. *280*, 908–924.
46. Muscutt, L.E., Dyke, G., Weymouth, G.D., Naish, D., Palmer, C., and Ganapathisubramani, B. (2017). The four-flipper swimming method of plesiosaurs enabled efficient and effective locomotion. Proc. R. Soc. Lond. B. Biol. Sci. *284*, 20170951.
47. Smith, A.S. (2013). Morphology of the caudal vertebrae in *Rhomaleosaurus zetlandicus* and a review of the evidence for a tail fin in Plesiosauria. Paludicola *9*, 144–158.
48. Sennikov, A.G. (2019). Peculiarities of the structure and locomotor function of the tail in Sauropterygia. Biol. Bull. *46*, 751–762.
49. Natali, L., Blasetti, A., and Crocetti, G. (2019). Detection of Lower Cretaceous fossil impressions of a marine tetrapod on Monte Conero (Central Italy). Cret. Res. *93*, 143–150.
50. Natali, L., and Leonardi, G. (2023). *Coneroichnus marinus* ichnogenus et ichnospecies nov., a fossil trackway of marine reptile in the Maiolica Formation (Upper Jurassic–Lower Cretaceous) from Monte Conero, Marche, Italy. Rev. Bras. Paleontol. *26*, 156–171.
51. Geister, J. (1998). Lebensspuren von Meersauriern und ihren Beutetieren im mittleren Jura (Callovien) von Liesberg, Schweiz. Facies *39*, 105–124.
52. McHenry, C.R., Cook, A.G., and Wroe, S. (2005). Bottom-feeding plesiosaurs. Science *310*, 75.
53. Amorocho, D.F., and Reina, R.D. (2007). Feeding ecology of the East Pacific green sea turtle *Chelonia mydas agassizii* at Gorgona National Park, Colombia. Endang. Species Res. *3*, 43–51.
54. Bowen-Stevens, S.R., Gannon, D.P., Hazelkorn, R.A., Lovewell, G., Volker, K.M., Smith, S., Tumlin, M.C., and Litz, J. (2021). Diet of Common bottlenose dolphins, *Tursiops truncatus*, that stranded in and near Barataria Bay, Louisiana, 2010–2012. Southeast. Nat. *20*, 117–134.
55. Bardet, N., and Fernandez, M. (2000). A new ichthyosaur from the Upper Jurassic lithographic limestones of Bavaria. J. Paleontol. *74*, 503–511.
56. Spindler, F., Lauer, R., Tischlinger, H., and Mäuser, M. (2021). The integument of pelagic crocodylomorphs (Thalattosuchia: Metriorhynchidae). Palaeontol. Electron. *24*, a25.
57. Troein, C., Siregar, S., Beeck, M.O.D., Peterson, C., Tunlid, A., and Persson, P. (2020). OCTAVVS: A graphical toolbox for high-throughput preprocessing and analysis of vibrational spectroscopy imaging data. Methods Protoc. *3*, 34.
58. Toplak, M., Birarda, G., Read, S., Sandt, C., Rosendahl, S.M., Vaccari, L., Demšar, J., and Borondics, F. (2017). Infrared Orange: connecting hyperspectral data with machine learning. Synchro. Rad. *30*, 40–45.
59. Toplak, M., Read, S.T., Sandt, C., and Borondics, F. (2021). Quasar: easy machine learning for biospectroscopy. Cells *10*, 2300.
60. Richardson, K.C., Jarett, L., and Finke, E.H. (1960). Embedding in epoxy resins for ultrathin sectioning in electron microscopy. Stain Technol. *35*, 313–323.

Please cite this article in press as: Marx et al., Skin, scales, and cells in a Jurassic plesiosaur, Current Biology (2025), https://doi.org/10.1016/j.cub.2025.01.001



CellPress
OPEN ACCESS

## STAR★METHODS

### KEY RESOURCES TABLE

| REAGENT or RESOURCE | SOURCE | IDENTIFIER |
|---|---|---|
| Software and algorithms | | |
| AZtecLive 6.1 | Oxford Instruments | https://nano.oxinst.com/products/azteclive |
| AZtecCrystal | Oxford Instruments | https://nano.oxinst.com/azteccrystal |
| OCTAVVS 0.1.22 | Troein et al.[57] | https://pypi.org/project/octavvs/ |
| OMNIC™ Spectra Software | Thermo Fischer Scientific | https://www.thermofisher.com/order/catalog/product/833-036200 |
| Quasar | Toplak et al.[58,59] | https://quasar.codes/ |
| SurfaceLab, version 7.1 | IONTOF GmbH | https://www.iontof.com/ |
| Biological samples | | |
| MH 7 fossilized tissue | This paper | MH 7 |
| *Dermochelys coriacea* | This paper | ZMUC-R2106; LO unnumbered |
| *Ctenochelys acris* | This paper | SMU 76353 |
| *Trachemys scripta elegans* | This paper | SMU R133 |
| *Caretta caretta* | This paper | ZMUC-KPC16030906 |
| *Varanus exanthematicus* | This paper | LO 10298 |

### METHOD DETAILS

#### Sample preparation

Samples of fossilized soft tissues from MH 7 were removed using hand tools and loosely wrapped in aluminum foil before being placed inside individual plastic containers that were rinsed with ultrapure water (Milli-Q) and sterilized with 96% ethanol (*Avantor* Inc., Radnor, USA). Following transport to LU, the samples were rinsed in Milli-Q water to remove adhering debris; they were then sterilized again in 96% ethanol. All sample handling was done with forceps rinsed with Milli-Q water and sterilized using either 70% or 96% ethanol.

Prior to destructive processing, all samples were photographed using an *Olympus* SC30 digital camera mounted on an *Olympus* SZX16 stereomicroscope, as well as an *Olympus* SZX10 stereomicroscope equipped with an *Olympus* SC50 digital camera. Samples selected for demineralization were then cut using a sterilized *Dremel*® saw and placed into sterile 5 mL jars before being rinsed with 96% ethanol and set to air dry on aluminum foil. The dried samples were then stored at 4° C in separate sterile 5 mL jars capped with aluminum foil.

#### TLM and thin-sectioning

For TLM, demineralized tail and forelimb skin samples were mounted onto Menzel Superfrost® Plus (*Thermo Scientific* Inc., Waltham, USA) glass slides with Menzel™ microscope cover slips (*Thermo Scientific* Inc., Waltham, USA) for observation using an *Olympus* BX51 fluorescence microscope with an *Olympus* DP74 digital camera. For petrographic thin-sectioning, non-demineralized/untreated tail and forelimb skin samples were embedded in a 5:1 mixture of Araldite DBF (*ABIC Kemi* AB, Norrköping, Sweden) epoxy casting resin and *Ren*™ HY 956 hardener (*Huntsman Corporation*, The Woodlands, USA), which was set to cure in an oven at 45–50° C for 24 hrs. The samples were then ground until transparent using 600 and 1200 grit resin-bonded diamond discs (*Struers* Inc., Ballerup, Denmark), and polished using polishing pads and diamond paste. Cyanoacrylate glue prevented breakage during grinding. Imaging of petrographic thin-sections was undertaken on an *Olympus* BX50 polarized light microscope equipped with an *Olympus* SC50 digital camera.

#### SEM, EDX, and EBSD

Prior to demineralization, forelimb skin samples were imaged at LU on a *TESCAN* Mira3 High Resolution Schottky Field Emission Gun Scanning Electron Microscope (FEG-SEM) under low vacuum and without coating. Working distance was 6–9 mm with an electron energy of 5 keV. EDX and EBSD of thin-sectioned skin samples was also carried out at LU with an *X-MaxN* 80 detector (124 eV, 80 $mm^2$) and a *NordlysNano* detector (*Oxford Instruments*, Abingdon, UK) attached to the FEG-SEM. EDX and EBSD used working distances of 16/19 mm and an electron energy of 20 keV for skin samples from dorsal/ventral sides of the tail, respectively. EDX and EBSD data was processed using *AZtecLive* 6.1 (*Oxford Instruments*, Abingdon, UK), with post-processing for removal of wild spikes using *AZtecCrystal* (*Oxford Instruments*, Abingdon, UK).

Please cite this article in press as: Marx et al., Skin, scales, and cells in a Jurassic plesiosaur, Current Biology (2025), https://doi.org/10.1016/j.cub.2025.01.001



FEG-SEM imaging was also undertaken at RISE Research Institutes of Sweden in Borås, Sweden. Tail and forelimb skin samples were imaged both before and after demineralization, and under high vacuum without coating using a *Zeiss* Supra 40VP FEG-SEM equipped with an Everhardt-Thornley type electron detector (SE2). The working distance was 3–5 mm, and the electron energy was 1–2 keV. EDX used *X*-Max 50 $mm^2$ detector (*Oxford Instruments*, Abingdon, UK) set at a working distance of 8.5 mm and an electron energy of 15 keV.

## IR microspectroscopy and ToF-SIMS

Our skin samples were separated into two subsets for demineralization: (1) those taken from the ventral and dorsal sides of the tail (N=2); (2) those taken from the ventral side of the tail and flipper (N=3). Demineralization of the subset (1) samples from the ventral side of the tail proceeded in a molecular biology grade ethylenediaminetetraacetic acid (EDTA) solution of 0.5 M and pH 8 (*AppliChem*, Darmstadt, Germany) for one week, during which the supernatant was replaced with fresh EDTA every other day. The samples were then washed by exchanging the supernatant with a Bioultra grade solution of 0.25 M ammonium formate (*Sigma-Aldrich*, St. Louis, USA) 14 times, and then rinsed six times with a solution of 0.15 M ammonium formate. After rinsing, pieces of the demineralized skin were pipetted onto two silicon wafers (*Sci-Mat Silicon Materials*, Kaufering, Germany) for ToF-SIMS analysis, and onto two $CaF_2$ windows (*Crystran* Ltd, Dorset, UK) for IR microspectroscopy; these were left to air dry. The $CaF_2$ window samples were placed in a vacuum chamber ($10^{-7}$ mbar) for 1.5 hrs to evaporate the ammonium formate salt ($NH_4HCO_2$). Additional rinsing in 15% aqueous sodium chloride (*Sigma-Aldrich*, BioXtra grade) was also performed to remove residual $NH_4HCO_2$ prior to IR microspectroscopy.

Demineralization of the subset (1) samples from the dorsal side of the tail took place in EDTA for 20 days with the supernatant being replaced every other day. This was followed by 20 rinses in Milli-Q water before drying on a $CaF_2$ window and sterile silicon wafer.

The subset (2) samples from the ventral side of the tail and the flipper were first inspected under a stereomicroscope to detect any residual glue. They were then placed in an EDTA solution (refreshed three times for the subset [2] flipper tissue samples) for 22 and 26 days, respectively. One of the subset (2) tail samples was then rinsed with 0.25 M NaCl and 0.15 M NaCl sequentially 10 times for each before being examined using IR microspectroscopy. The other subset (2) tail sample was rinsed in 0.25 M ammonium formate and 0.15 M ammonium formate 10 times for each prior to ToF-SIMS analysis. The subset (2) flipper samples were rinsed 10 times with 0.25 M ammonium formate, and six times in 0.15 M ammonium formate before ToF-SIMS examination.

IR microspectroscopic measurements were undertaken at the SOLEIL synchrotron facility in France, and independently at LU. SOLEIL used a *Nicolet Continuum* FT-IR microscope (*Nicolet CZ*, Prague, Czech Republic) with a synchrotron light source in transmission mode. IR spectra were visualized and studied using both *OMNIC*™ Spectra Software and *Quasar*.[58,59] LU used a *Hyperion* 3000 IR microscope coupled to a *Tensor* 27 spectrometer (*Bruker* Corp., Billerca, USA). IR spectra were recorded in transmission mode using a Focal Plane Array detector with 64 × 64 elements. They were constructed from 1024 averaged scans and corrected for atmospheric contributions from $CO_2$ and $H_2O$ using rubber band baseline correction in *OCTAVVS* v.0.1.22.[57]

ToF-SIMS was carried out at RISE on a TOFSIMSIV instrument (*IONTOF* GmbH, Münster, Germany) using 25 keV $Bi_3^+$ primary ions and low-energy electron flooding for charge compensation. Positive and negative ion data were acquired in the static SIMS regime (accumulated primary ion dose density kept below $3 \times 10^{12}$ $cm^{-2}$), with optimization for either high mass resolution (bunched mode, $m/\Delta m \approx 5{,}000$, lateral resolution 3–5 μm) or high image resolution ($m/\Delta m \approx 300$, lateral resolution 0.5–1 μm). Spectra and images were generated using *SurfaceLab* v.7.1 (*IONTOF* GmbH, Münster, Germany). Mass spectra of the glue and surrounding rock matrix were measured as controls to compare with spectra from the fossilized soft tissues.

## Comparative samples

Our comparative samples included carapace scutes from the fossil sea turtle, *Ctenochelys acris* (Southern Methodist University, USA [SMU] 76353), and the extant Red-eared slider turtle, *Trachemys scripta elegans* (SMU R133), flipper skin from a juvenile Loggerhead turtle, *Caretta caretta* (University of Copenhagen Zoological Museum, Denmark [ZMUC]-KPC16030906), dorsal body skin from an adult Savannah monitor, *Varanus exanthematicus* (Department of Geology, Lund University, Sweden [LO] 10298), flipper skin from a juvenile Leatherback turtle, *Dermochelys coriacea* (ZMUC-R2106), and carapace and eyelid skin from an adult *D. coriacea* (LO unnumbered sample provided by Marine Turtle Permit 073 from the US Fish and Wildlife Service and Florida Fish and Wildlife Conservation Commission).

Scute tissue was removed from SMU 76353 using hand tools and demineralized before being stored in EDTA for an extended period of time. The samples were then mounted on SEM stubs for imaging at RISE using a *Zeiss* Supra 40VP FEG-SEM equipped with an Everhardt-Thornley type electron detector (SE2).

Untreated scute tissue from SMU R133 was coated with a 15 nm thick AuPd film prior to imaging at RISE on a *Zeiss* Supra 40VP FEG-SEM equipped with an Everhardt-Thornley type electron detector (SE2).

Flipper skin from ZMUC-KPC16030906 and ZMUC-R2106 were fixed in 2.5% glutaraldehyde and 70% ethanol, respectively. They were then sectioned using a sterile scalpel and imaged using an *Olympus* SZX10 stereomicroscope equipped with an *Olympus* SC50 digital camera.

Dorsal body skin from LO 10298 was fixed in 4% Sörensen phosphate buffered formalin (pH 7.2). The tissue was then embedded in EPON (*Agar Scientific*, Stansted, UK) and stained with Richardson's solution (methylene blue and Azure II)[60] before being cut into 3 μm sections with a *Leica* UC7 ultramicrotome. Imaging used an *Olympus* BX35 polarized light microscope equipped with an *Olympus* UC30 digital camera.

Please cite this article in press as: Marx et al., Skin, scales, and cells in a Jurassic plesiosaur, Current Biology (2025), https://doi.org/10.1016/j.cub.2025.01.001





The LO unnumbered *D. coriacea* carapace and eyelid skin were fixed overnight using 2.5% glutaraldehyde and 2% paraformaldehyde in a 0.1 M sodium cacodylic buffer solution. They were then post-fixed using 2% osmium tetroxide in distilled water at 7° C for 1 hr. Dehydration used a graded ethanol series of 70% for 2 × 10 min, 96% for 2 × 10 min, and 100% for 2 × 15 min before being embedded in *Agar* 100 resin (*Agar Scientific*, Stansted, UK) with acetone. Ultrathin sections were cut using a *Leica* UC7 ultramicrotome to 50 nm for the carapace skin, and 1 μm for the eyelid skin which was stained with Richardson's solution[60] and imaged using an *Olympus* BX35 polarized light microscope equipped with an *Olympus* UC30 digital camera. The carapace skin sections were mounted on copper grids and stained with 2% uranyl acetate for 30 min, and Reynolds lead citrate for 3 min before imaging using a *JEOL* 1400 Plus Transmission Electron Microscope at 100 kV equipped with a CMOS camera.

**Current Biology, Volume *35***

## Supplemental Information

# Skin, scales, and cells in a Jurassic plesiosaur

**Miguel Marx, Peter Sjövall, Benjamin P. Kear, Martin Jarenmark, Mats E. Eriksson, Sven Sachs, Klaus Nilkens, Michiel Op De Beeck, and Johan Lindgren**

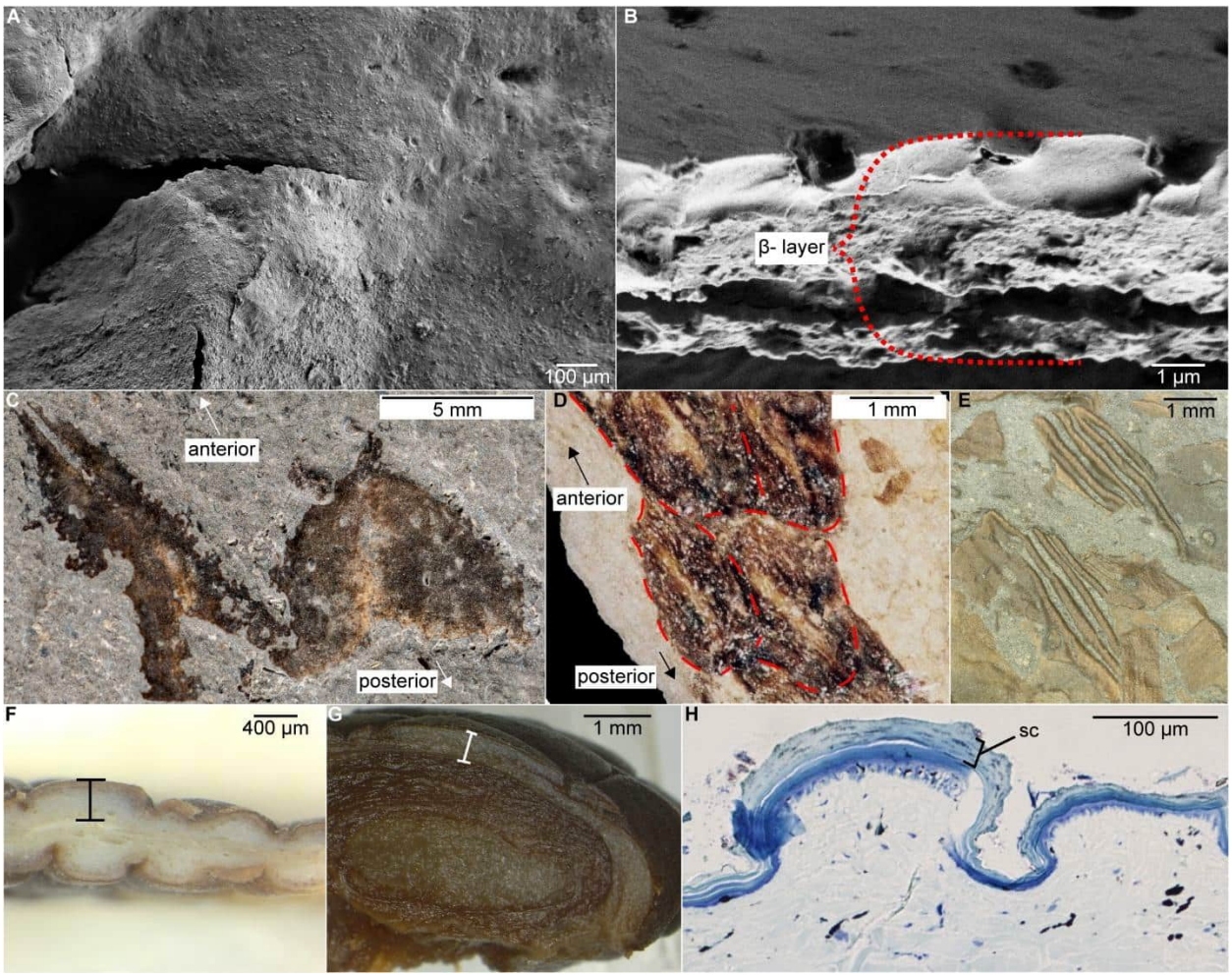


**Figure S1**. **Preserved plesiosaur scales from MH 7 and comparative reptile tissues, related to Figure 3.**

(A) SEM image enlargement of a demineralized carapace scute from the fossil sea turtle, *Ctenochelys acris* (SMU 76353), showing smooth surface texture.

(B) SEM image of the stratified carapace scute layers in the extant Red-eared slider turtle, *Trachemys scripta elegans* (SMU R133). Outermost β-layer is composed of multiple corneous sub-layers.

(C) Scales from the trailing edge of the flipper in MH 7.

(D) Scales (red dashed lines) from the extinct mosasauroid marine lizard, *Plotosaurus bennisoni* (University of California Museum of Paleontology [UCMP] 152664).

(E) Scale-less skin from the extinct ichthyosaur, *Stenopterygius* sp. (MH 432), showing folds produced by de-tensioning of the soft tissue structure during decomposition.

(F) Cross-section through the flipper trailing edge of a juvenile Leatherback turtle, *Dermochelys coriacea* (ZMUC-R2106); black line = skin thickness.

(G) Cross-section through the flipper leading edge of a Loggerhead turtle, *Caretta caretta* (ZMUC-KPC16030906); white line = skin thickness.

(H) Histological section through the scaly back skin of a Savannah monitor, *Varanus exanthematicus* (LO 10298) showing the thickened stratum corneum; sc = stratum corneum.

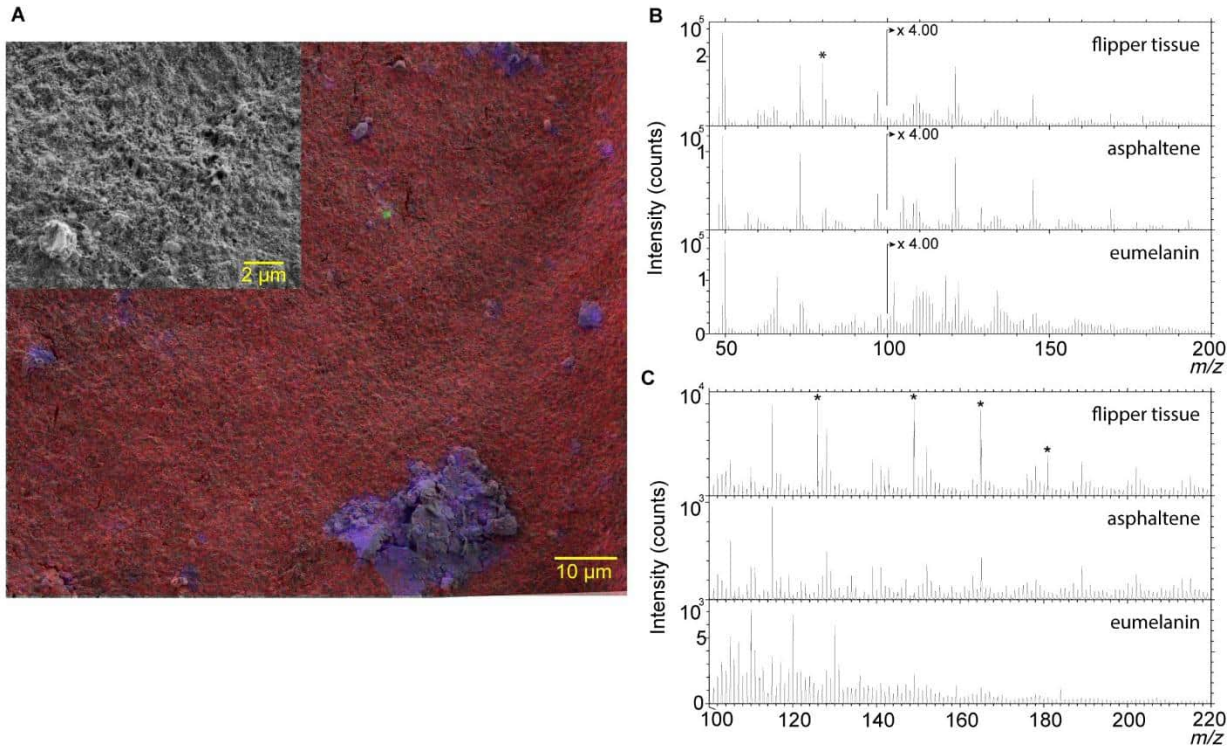


**Figure S2. ToF-SIMS analysis of scales from the forelimb trailing edge in MH 7, related to Figure 3.**
(A) Superimposed ToF-SIMS and FEG-SEM images of the scale surface. ToF-SIMS overlay image shows the detected intensity of ions representing: red = polycyclic aromatic hydrocarbons (PAHs) ($C_4H^-$ + $C_6H^-$); green = glue (*m*/z 112 + *m*/z 177); blue = silica ($SiO_2^-$ + $SiO_3^-$). Inset is an SEM image of the fossil surface without the overlay.
(B) Negative-ion and (C) positive-ion spectra from (top) the fossil surface at a region of interest (ROI) with high PAH signal, (center) asphaltene[S1], and (bottom) *Sepia* eumelanin. Asterisks indicate peaks associated to alkali sulfate.

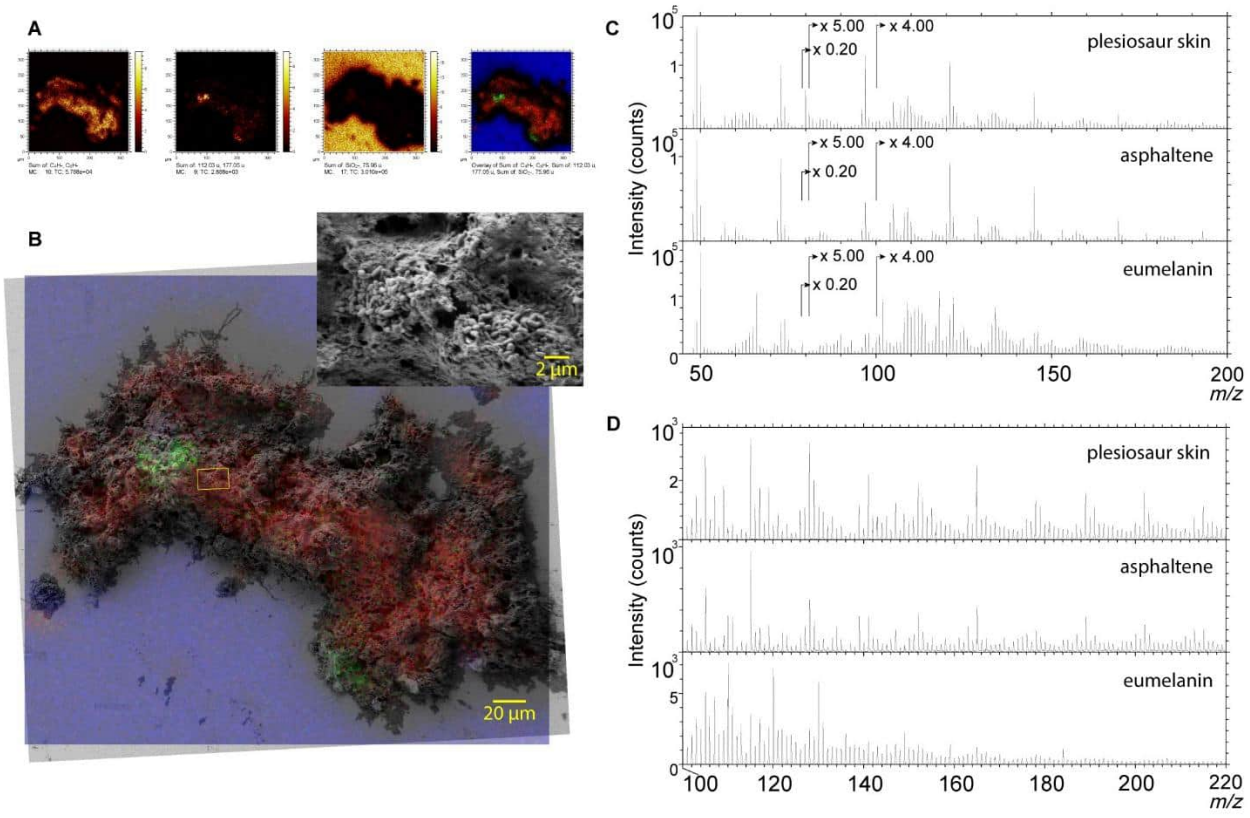


**Figure S3. ToF-SIMS analysis of skin from the ventral side of the tail in MH 7, related to Figure 2.**
(A) ToF-SIMS images of negative ions with an overlay representing: red = polycyclic aromatic hydrocarbons (PAHs) ($C_4H^-$ + $C_6H^-$); green = glue (*m*/z 112 + *m*/z 177); blue = silica ($SiO_2^-$ + $SiO_3^-$).
(B) FEG-SEM image of the demineralized fossil tissue with a ToF-SIMS overlay from (A). Inset shows a magnified FEG-SEM image of the fossil tissue with remnant melanosomes aggregates.
(C) Negative-ion and (D) positive-ion spectra from (top) the fossil surface at an ROI with high PAH signal, (center) asphaltene[S1], and (bottom) *Sepia* eumelanin.

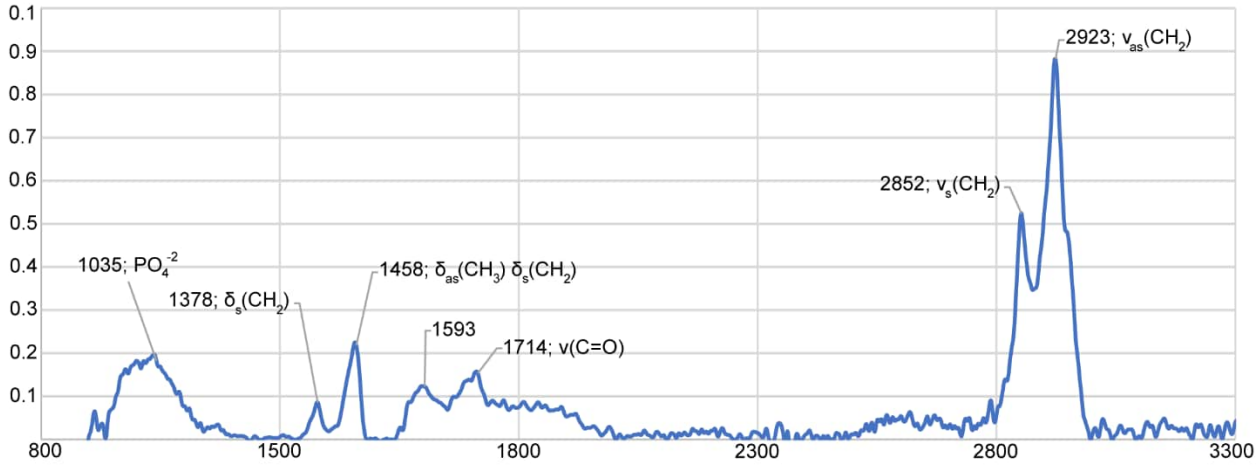


**Figure S4. IR microspectroscopic measurements of skin from the ventral side of the tail in MH 7, related to Figure 2.**
The wavelength peak at 1035 $cm^{-1}$ indicates phosphate from the fossil sample. All other peaks represent organic remains, predominantly hydrocarbons. Vibration modes: as = asymmetric; δ = deformation; s = symmetric; *v* = stretching.

**SUPPLEMENTARY REFERENCE**

S1. Lu, X., Soenen, H., Sjövall, P., and Pipintakos, G. (2021). Analysis of asphaltenes and maltenes before and after long-term aging of bitumen. Fuel. *304*, 121426.